Morphological Development in Alkyl-Substituted Semiflexible Polymers

J. L. Lee, E. M. Pearce, and T. K. Kwei*

Department of Chemical Engineering, Chemistry, and Materials Science, Polytechnic University, Six Metrotech Center, Brooklyn, New York 11201

Received May 8, 1997; Revised Manuscript Received September 16, 1997[⊗]

ABSTRACT: Nonsymmetrically substituted semiflexible polymers were synthesized by reacting (hydroxypropyl)cellulose (HPC) with hexyl, octyl, dodecyl, and octadecyl isocyanates. X-ray diffraction studies indicate that the polymer chains are assembled in regular, layered arrays. Polymers with six and eight carbons in the side chains (C6HPC and C8HPC) showed spherulitic structures typical of common crystalline polymers when examined by a polarized optical microscope (POM), whereas liquid crystalline (LC) textures were observed for C12HPC and C18HPC. When the polymers were slowly cooled from the melt, crystalline (C) textures could be obtained for C12HPC and C18HPC at preselected temperatures slightly higher than the corresponding (isotropic → LC) transition temperatures determined by DSC cooling scans. Upon further cooling, liquid crystalline structures appeared at temperatures 5−6 °C lower. The unusual POM observations are in contrast to conventional thermal transitions reported for liquid crystalline polymers, where the isotropic → LC transition takes place at a temperature higher than that of the LC → C transition, but are consistent with Keller's studies on another liquid crystalline polymer.

Introduction

Comb-type polymers containing long alkyl side groups were studied as early as 1964.[1] Wide-angle X-ray scattering (WAXS) investigations on poly(*n*-alkyl acrylates),[2,3] poly(*n*-alkyl methacrylates),[4,5] and poly(acrylamides) and their copolymers[5] suggested that in spite of the different chemical structures, the flexible main chains seemed to be able to arrange themselves in regular, layered arrays.

The melting (T_m) and the isotropization temperatures (T_i) of rigid polymers such as aromatic polyesters,[6−10] polyamides,[11−14] polyimides,[8] polythiophenes,[15−17] and polyanilines[18] were markedly decreased by attaching long alkyl side chains. Layered structures prevailed in all the alkyl-substituted rigid polymers. The *d* spacing in the *a*-axis direction (distance between the main chains) increased linearly with *n* (the number of carbon atoms in the side chain) for most of the mono- and disubstituted polymers but showed a less regular increment for highly substituted polymers (two or more alkyl substituents on each ring).

The primary purpose of this study is to investigate the effects of the alkyl side chains on the morphology of a semiflexible polymer. The polymer of our choice is (hydroxypropyl)cellulose (HPC), which is inherently semiflexible due to the ether linkage between mesogens. In addition, HPC is crystallizable. Its lyotropic and thermotropic characteristics have been well documented. Although the lyotropic properties of many alkyl-substituted cellulosic polymers were reported by Gray[19,20] and by Glasser,[21,22] their thermotropic properties have not been thoroughly investigated. In this regard, HPC is a good vehicle for such studies. By reacting all the hydroxyl groups, we can arrive at a structure in which three long substituents are located nonsymmetrically on each ring. The liquid crystalline (LC) morphologies of such novel chemical structures have not been studied in the past. In an earlier paper,[23] we reported on side-chain crystallization in the alkyl-substituted HPC's. The morphologies and thermotropic properties of these polymers are the subjects of investigation in this report.

Experimental Section

Synthesis and Characterization of C*n*HPC's. HPC derivatives were synthesized by reacting (hydroxypropyl)-cellulose with hexyl, octyl, dodecyl, and octadecyl isocyanates in anhydrous pyridine with a moderate amount of dibutyltin dilaurate as the catalyst. The synthesis of C*n*HPC's was described in an earlier publication.[23] Elemental analysis and infrared and NMR spectroscopies were employed to characterize the structure of the polymers.[23]

Wide-Angle X-ray Scattering (WAXS). X-ray diffraction patterns were obtained from a Philips 3100 X-ray generator with a Philips APD-3720 diffractometer, in which the high-intensity monochromatic Cu Kα_1 radiation (Cu Kα_1 = 1.5406 Å) was generated. In addition to the bulk C*n*HPC's in the powder form made by grinding the samples in liquid nitrogen, solvent-cast samples were obtained by casting the individual C*n*HPC's/$CHCl_3$ solution on a glass slide followed by slow evaporation of the solvent. To study the shear and cooling rate effects, bulk samples were heated on a hot stage (Mettler FP82) and manually sheared in the molten state, followed by various cooling processes to form homogeneous thin films.

Differential Scanning Calorimetry (DSC). DSC studies were carried out on a TA 2920 Modulated DSC. About 5 mg of each sample was used in the heating/cooling cycle experiments conducted at 10 °C/min under nitrogen.

Polarized Optical Microscopy (POM). An optical microscope (Nikon Optiphot) equipped with crossed polarizers and a hot stage was used to observe the morphological features and phase transitions of the polymers. Aside from the solvent-cast samples, sheared samples were prepared by the same methods as described in the WAXS experiments.

Results

Wide-Angle X-ray Scattering. The WAXS profiles of the bulk HPC derivatives are shown in Figure 1. Since the reflections in the wide-angle region (2θ = 15−30°) were already discussed in a previous publication[23] in relation to side-chain crystallization, only the results in the low-angle region (2θ = 2−16°) will be examined in this paper. C6HPC exhibited a strong diffraction peak at d = 17.2 Å and a weak signal at d = 5.6 Å (third-

[⊗] Abstract published in *Advance ACS Abstracts,* December 1, 1997.

S0024-9297(97)00647-5 CCC: $14.00

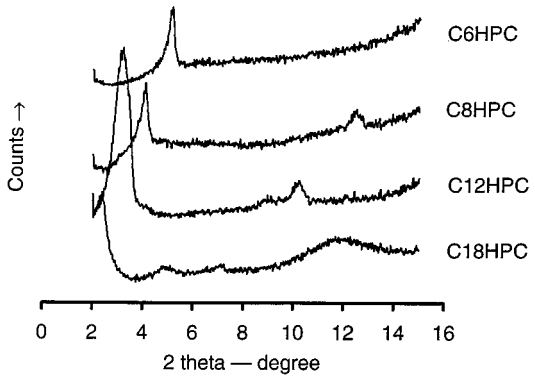

Figure 1. WAXS profiles of bulk C*n*HPC samples.

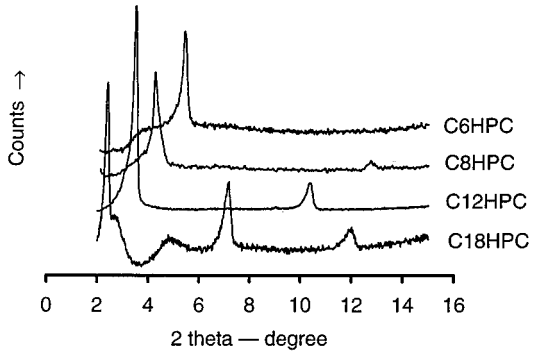

Figure 2. WAXS profiles of C*n*HPC's cast from $CHCl_3$.

order reflection) in this region. Similar diffraction patterns (a strong primary reflection together with a weaker third-order peak) were observed for C8HPC and C12HPC with *d* values of 21.7/7.1 Å for the former and 27.6/8.6 Å for the latter. However, a significantly different X-ray profile was obtained for C18HPC. Diffraction peaks at 37.1, 18.2, and 12.4 Å were identified as the first-, second-, and third-order reflections, respectively; note that the second-order reflection was absent in all other HPC derivatives. In addition, a broad peak was located at 7.4 Å. Although the spacing is one-fifth that of the first-order reflection, the peak intensity is unexpectedly high compared to the third order and its assignment requires additional study. For the purpose of comparison, solvent-cast samples were also examined (Figure 2). C6HPC exhibited a strong reflection at $d = 16.5$ Å and a weak signal at $d = 5.5$ Å (third-order reflection). C8HPC displayed a similar pattern with *d* values of 21.3 and 7.1 Å (third-order reflection). For C12HPC, in addition to the peaks at $d = 25.7$ and 8.5 Å (third order), a fifth-order reflection at $d = 5.1$ Å was present. The X-ray profile of solvent-cast C18HPC showed notable differences from that of the bulk sample. The second-order reflection at $d = 18.5$ Å was still observed; the peak intensity, however, was weaker than that of the third reflection at 12.4 Å. Interestingly, for the solvent-cast C18HPC, the fifth-order reflection with the unusually high intensity in the as-prepared sample now was weaker than the third-order reflection, in line with intuitive expectation. Furthermore, a faint peak at $d = 5.3$ Å (possibly seventh order) was also found. The *d* spacings of each sample are listed in Table 1.

The sheared C12HPC and C18HPC samples were cooled from the molten state by three different processes: (1) slow cooling immediately after being sheared, (2) annealing at the molten state for 10 min after shearing followed by slow cooling, and (3) annealing followed by fast cooling at a rate of ca. 50 °C/min. The results are listed in Table 2.

The sheared C12HPC which had been slowly cooled (process 1) exhibited the strongest peak intensities (Figure 3a). However, the various cooling processes did not change the peak positions to any significant extent in the low-angle region. Odd-number reflections were still observed and the corresponding *d* spacings were very close in all three samples, except that the fifth-order diffraction peak was not observed in process 3.

Shearing the melt also influenced the morphology of C18HPC. For the sample subjected to process 1, a primary reflection at 39.5 Å was observed, together with a peak at 35.5 Å. In addition, a well-developed second-order reflection was seen in the low-angle region. The third- and the fifth-order reflections were also clearly visible; the latter peak at 8.4 Å appeared only in process 1 for this series. Reheating the above sample to the isotropic state for a period of time followed by slow cooling (process 2) made the peak at 35.5 Å more prominent and drastically reduced the intensity of the previously observed strong reflection at 39.5 Å. Interestingly, a well-ordered pattern was still retained in the low-angle region, in which the primary reflection was stronger than the second-order reflection, which was in turn stronger than the third-order reflection. Fast cooling of the annealed sample (process 3) brought the first-order reflection to 38.6 Å, but higher order peaks were absent. Figure 3b shows the X-ray diffraction profiles of the thermally treated C18HPC's.

DSC Studies of C*n*HPC's. Figure 4 shows the thermograms of C*n*HPC's cooled from the melt and those of the subsequent heating (second heating scan) at a rate of 10 °C/min. C6HPC and C8HPC displayed a crystallization exotherm (T_{exo}) at 39 and 60 °C, respectively, when cooled from the molten state. In the subsequent heating scan of C6HPC, a glass transition (T_g) at −19 °C, a cold crystallization exotherm at 7 °C, and a melting transition (T_m) at 68 °C were seen. Similarly, a glass transition at −23 °C, a cold crystallization at 15 °C, and a melting transition at 82 °C were observed for C8HPC. C12HPC exhibited an exotherm at 93 °C in the cooling scan and an isotropic melting at 106 °C in the heating scan. C18HPC responded similarly to the heating/cooling cycle, except for the observation of side-chain melting and crystallization.[23] The thermal transitions of the HPC derivatives are compiled in Table 3.

Polarized Optical Microscopy. The morphologies of the HPC derivatives were also studied by crossed polarized optical microscopy. In order to compare optical observations with the data obtained from WAXS

Table 1. *d* Spacing (Å) vs Side-Chain Length (*n*) of HPC Derivatives

	bulk samples				solvent-cast samples			
reflctn order	C18HPC	C12HPC	C8HPC	C6HPC	C18HPC	C12HPC	C8HPC	C6HPC
first	37.1	27.6	21.7	17.2	36.8	25.7	21.3	16.5
second	18.2				18.5			
third	12.4	8.7	7.1	5.6	12.4	8.5	7.1	5.5
fifth	7.4(?)				7.4	5.1		
seventh					5.3			

Table 2. *d* Spacing of the Sheared Samples with Various Cooling Processes[a]

	C12HPC			C18HPC				
				process 1		process 2		
reflctn order	process 1	process 2	process 3	1st set	2nd set	1st set	2nd set	process 3
first	29.6	29.9	29.1	39.5(s)	35.5(w)	39.5(vw)	35.2(s)	38.6
second					18.0		17.9	
third	9.9	9.8	9.5	13.9		13.9		
fifth	5.9	5.9		8.4				

[a] Process 1: slow cooling without annealing. Process 2: slow cooling after 10 min of annealing. Process 3: fast cooling (ca. −50°C/min) after 10 min of annealing. S: strong. W: weak. VW: very weak.

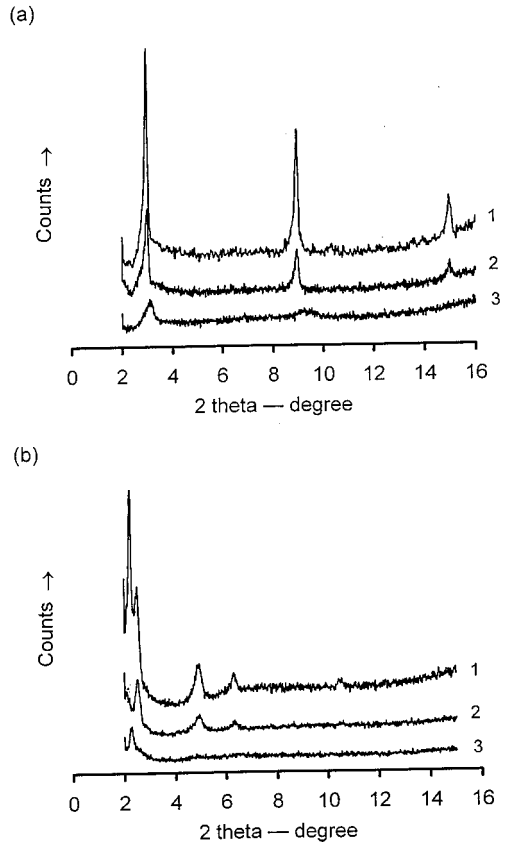

Figure 3. WAXS profiles of the sheared C12HPC (top set) and C18HPC (bottom set). The three curves in each set are the reflections with processes 1, 2, and 3 (from top to bottom).

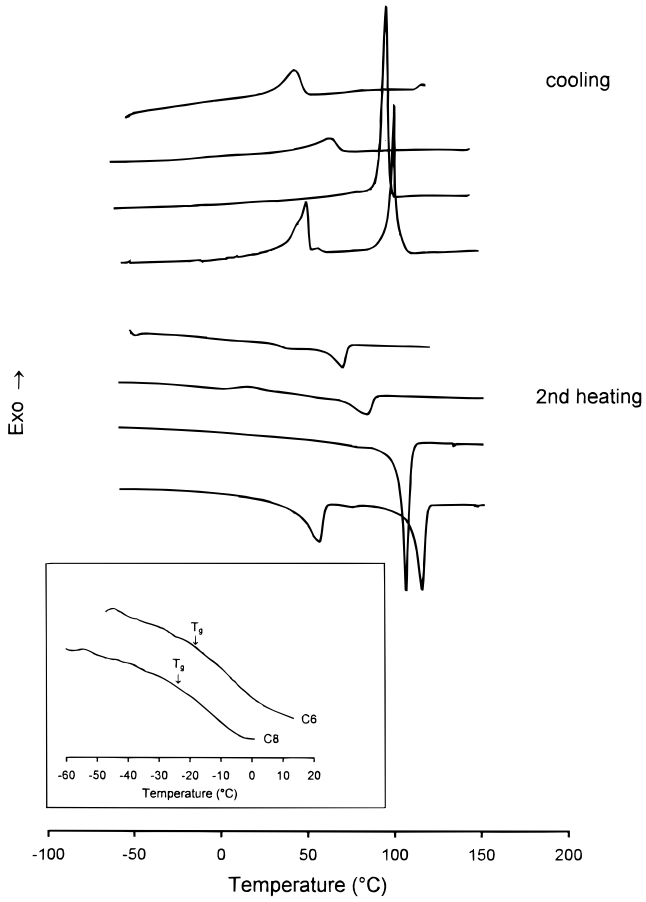

Figure 4. DSC thermograms of C*n*HPC's at a rate of 10 °C/min. The four curves in each set are C6-, C8-, C12-, and C18HPC, respectively (from top to bottom).

studies, two sets of samples were prepared, namely, solvent-cast C*n*HPC films and sheared samples of C12HPC and C18HPC.

Solvent-Cast Films. The homogeneity of the solvent-cast film depended on the solubility of each polymer and the rate of solvent evaporation. The morphologies of our samples seen by POM were not always the volume-filling type, and distinct features were often observed clearly only in certain portions of the samples, for example, near the edges of the samples.

Crossed polarized optical micrographs of solvent-cast C*n*HPC's are shown in Figure 5. C6HPC and C8HPC each displayed a crystalline morphology. The size of the spherulites varied from one spot to another in the sample. A coarse ring pattern inside the C6HPC spherulites was readily observed. C8HPC exhibited a fine fibrillar texture; a sheaflike structure (hedrite) was also seen at various spots. C12HPC had a branched lamellar structure, Figure 5c, whereas for C18HPC, the bright birefringence embedded in the amorphous background indicated a mottled texture, Figure 5d.

Sheared C12HPC and C18HPC. To elucidate the effect of shear stress on the development of polymer

Table 3. Thermal Transitions of C*n*HPC's

	T_g, °C		T_s, °C		T_{exo}	T_i/T_m, °C	
	first heat	second heat	first heat	second heat	cooling, °C	first heat	second heat
C6HPC	−8	−19			39	70	68
C8HPC	−7	−23			60	90	82
C12HPC			45		93	106	106
C18HPC			52/58	56	97	115	115

morphology, both C12HPC and C18HPC were sheared in the molten state and cooled in accordance with procedures which were coincident with the cooling processes adopted in the WAXS studies. In addition, another cooling process was employed in which the samples were step-cooled from the isotropic state in such a manner that the samples were isothermally kept at preselected temperatures slightly above the major T_{exo} in the DSC cooling scans.

After the C12HPC sample was melted on the hot stage, a positive-birefringent "spherulite-like" structure, Figure 6a, developed upon slow cooling to room tem-

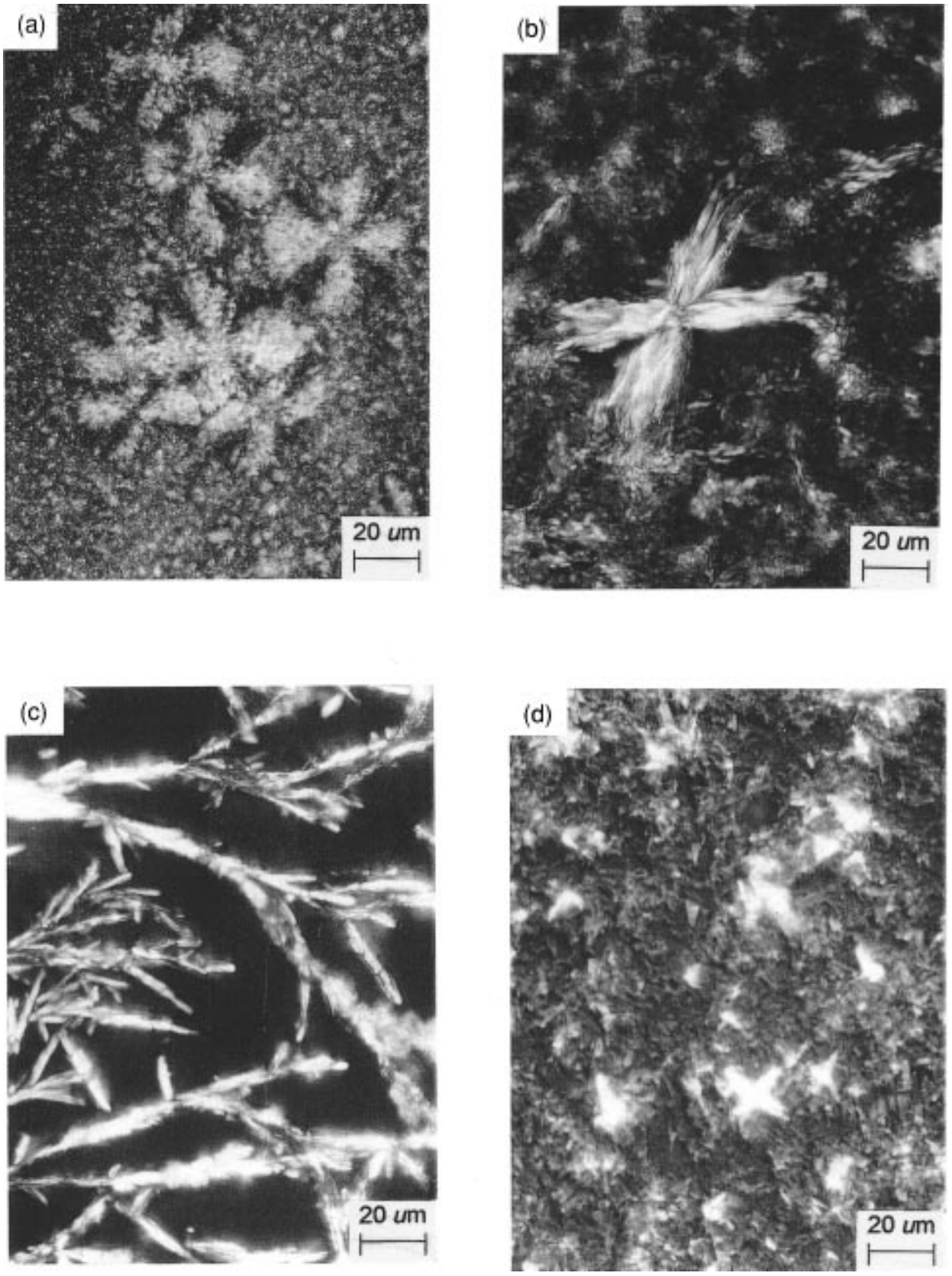

Figure 5. Optical micrographs of solvent-cast C*n*HPC's at 25 °C, 400×. (a) C6HPC, (b) C8HPC, (c) C12HPC, and (d) C18HPC.

perature (process 1 in the WAXS experiments). When the spherulite-like structure was reheated to the isotropic state followed by very slow cooling *(0.5 °C/min per step, 10 min at each step)* to ca. 100 °C, a leaflike structure developed, Figure 6b. As the step-cooling process continued, the intensity of birefringence of the leaflike structure increased. A second structure became visible at 94 °C and quickly filled the rest of the sample. Although there was a continuous increase in birefringence intensity, the texture did not change further as the sample was step-cooled to room temperature, Figure 6d. This second structure melted at 102 °C upon

Figure 6. Optical micrographs of sheared C12HPC. (a) Slowly cooled from the isotropic state to 25 °C, 400×; (b) reheated sample a to isotropic state followed by step-cooled to 99 °C, 300×; (c) step-cooled sample b to 90 °C, 300×; (d) step-cooled sample c to 25 °C, 300× (see text for step cooling).

reheating, but the leaflike structure remained. A further increase in temperature transformed the entire sample to the isotropic state at ca. 106 °C.

As would be expected, cooling rates influenced the morphology development. When fast-cooled from the isotropic state (process 3), C12HPC displayed a Schlieren structure, Figure 7a. Controlled cooling of the sample at a rate of 10 °C/min from the isotropic state led to a combination of the leaflike and the second structure, Figure 7b, but the thus obtained leaflike

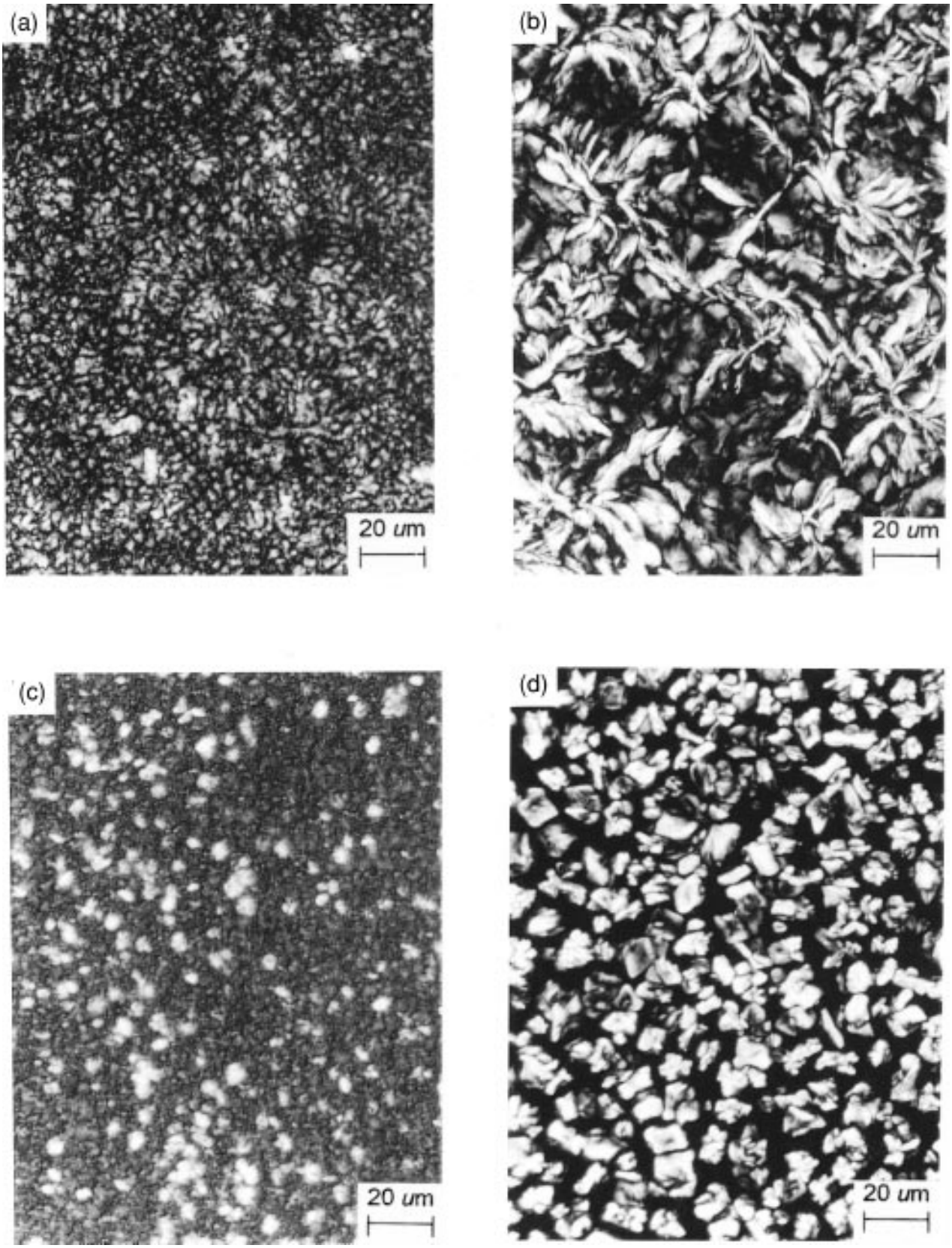

Figure 7. Optical micrographs of C12HPC and C18HPC cooled from the molten state to 25 °C, 400×. (a) C12HPC fast-cooled; (b) C12HPC cooled at −10 °C/min; (c) C18HPC fast-cooled; (d) C18HPC cooled at −10 °C/min.

structure was smaller in size and visually less ordered. These observations are summarized in Scheme 1.

C18HPC manifested a typical nematic structure[24] after the sheared sample had been slowly cooled (process 1) from the isotropic state, Figure 8a. After the nematic structure was destroyed by heating to the isotropic state and the molten sample was step-cooled to 109 °C, axialites were seen, Figure 8b. Nematic domains appeared when the sample was cooled further by the stepwise procedure to 102 °C, Figure 8c, although the structure was less perfect than that seen in the sheared sample at room temperature, Figure 8a. Similar to the observation in C12HPC, the texture did not change but the axialites and nematic structure continued to grow

Scheme 1. Optical Microscopy Observation of C12HPC

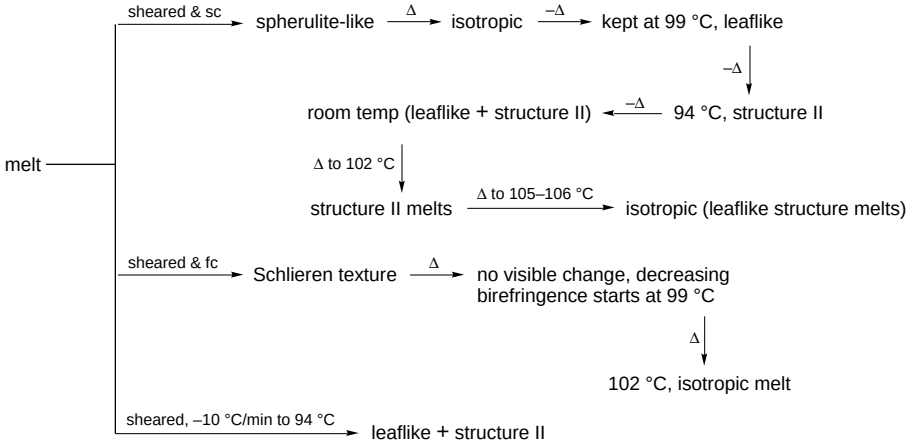

Scheme 2. Optical Microscopy Observation of C18HPC

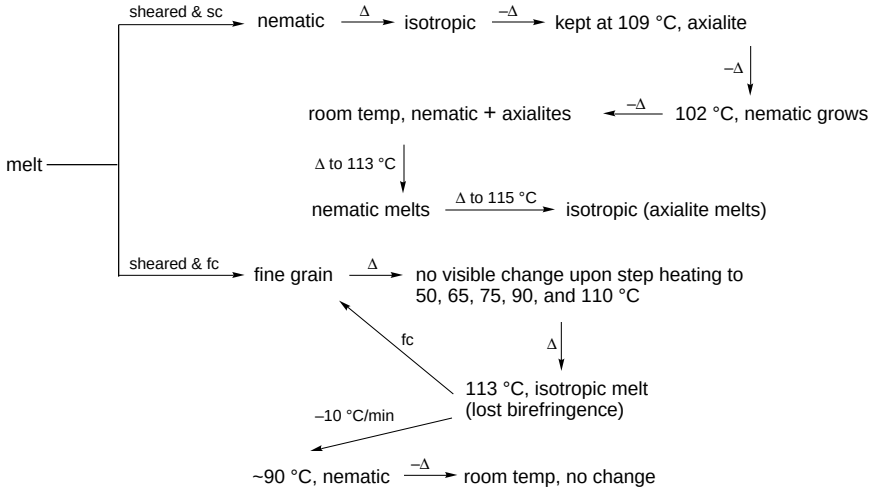

as the temperature was lowered to 25 °C, Figure 8d. Reheating the sample resulted in the disappearance of the nematic structure at ca. 113 °C at which the axialites remained intact. Isotropization occurred at 115−116 °C. Fast cooling of the molten C18HPC resulted in a completely different morphology. The mottled texture in Figure 7c was also liquid crystalline,[25] although the detailed features were too small to be seen by POM. On the other hand, nematic morphology was observed if the sample was cooled at a rate of 10 °C/min, Figure 7d. Scheme 2 outlines the POM observation for the sheared C18HPC.

Discussion

Layered Structures of C*n*HPC's. (a) Bulk and Solvent-Cast C*n*HPC's. In the low-angle region of the WAXS profiles, all C*n*HPC's (both bulk samples and solvent-cast) displayed odd-order reflections only, except for C18HPC in which the second-order reflection was clearly observed. This reinforced odd-order diffraction pattern had been observed in substituted rigid polymers[9,12] with four alkyl chains distributed on two aromatic rings in each repeating unit. In addition, the diffraction pattern of layered A−B-type diblock copolymers also showed odd-order reinforcement.[26] However, the intensities of the odd-order peaks in our case could not be explained by the theoretical calculation for diblock copolymers.

For the as-prepared C18HPC, the primary diffraction peak together with its higher order reflections demonstrated unambiguously the formation of a well-defined layered structure.[7−9] On the other hand, the second-order reflection in the solvent-cast C18HPC was weaker than the third order. Similar observations were reported in substituted aromatic polyesters[9] and polyamides[12] when the lengths of the four alkyl side chains are sufficiently long. In comparing the bulk and solvent-cast samples (Table 1), it is clear that, in films cast from a good solvent such as $CHCl_3$, the polymer chains were packed in a more regular fashion than in the bulk samples which were prepared by precipitating from a nonsolvent, due to the fact that the higher order reflections (the fifth in C12HPC and the seventh in C18HPC) were all observed in the solvent-cast species.

Wegner proposed a bilayer model[9] in which the main chains were aligned in a zigzag pattern (Figure 9a) and the side chains were not interdigitated but were tilted at an angle to the main chain (Figure 9b). This bilayer model appears to be applicable to our results for the following reasons. The alkyl side chains of C*n*HPC's most likely are not interdigitated since the side chains on the C2 and C3 positions were so close to each other that there would be insufficient space to accommodate another incoming alkyl chain from the opposite direction. In addition, the *d* spacing between main chains (*a*-axis direction) supports the above assumption, as we shall explain in the following. For the mono- and disubstituted rigid polymers, the increment in the *d* spacing for each CH_2 was about 0.8−1.25 Å in the literature. In our polymers, the average increment in *d* spacing per CH_2 unit was 1.66 Å, much greater than the theoretical value of 1.25 Å for each CH_2 contribution

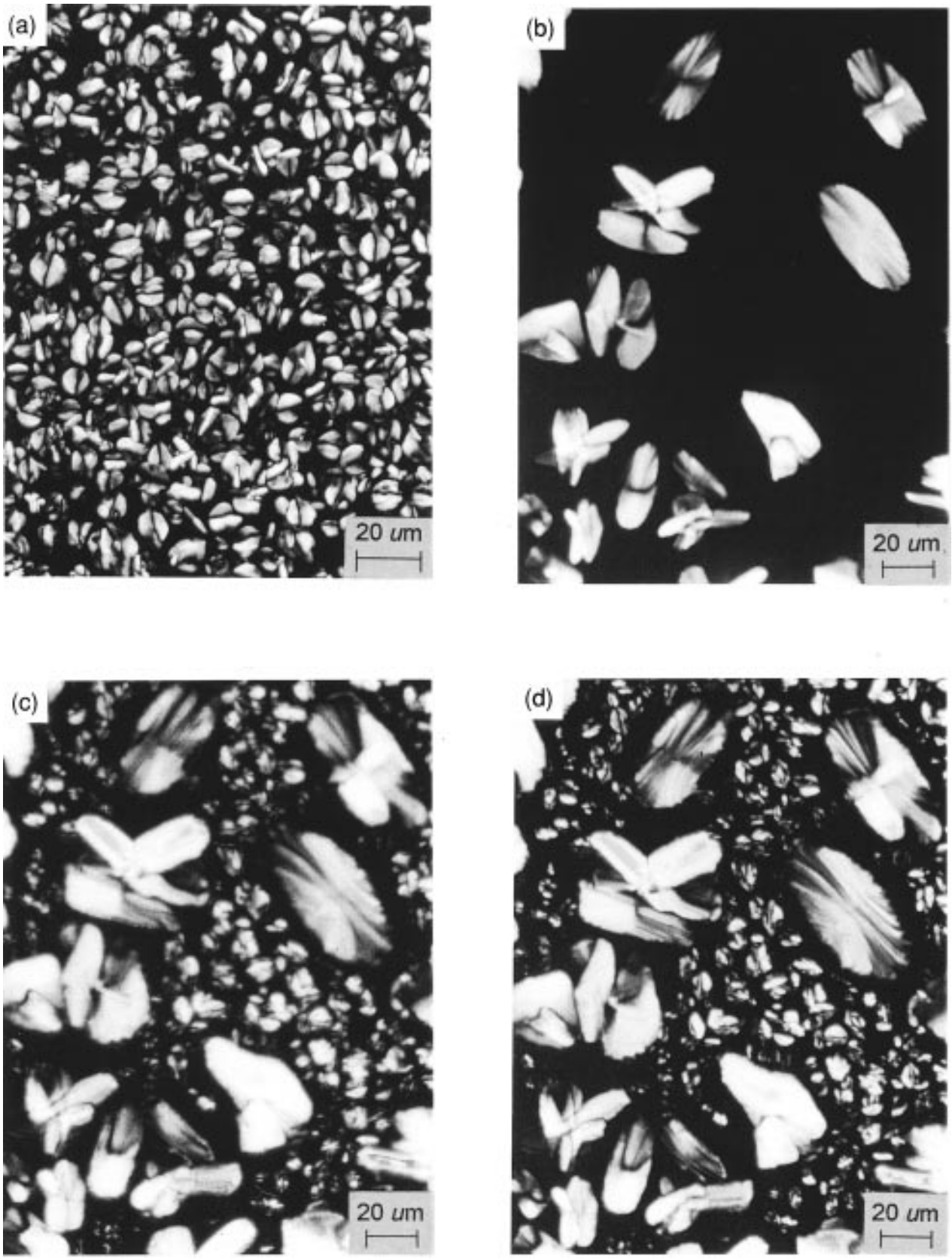

Figure 8. Optical micrographs of sheared C18HPC. (a) Slowly cooled from the isotropic state to 25 °C, 400×; (b) reheated sample a to isotropic state followed by step-cooled to 109 °C, 300×; (c) step-cooled sample b to 50 °C, 300×; (d) step-cooled sample c to 25 °C, 300× (see text for step cooling).

in intercalated side chains, again consistent with non-interdigitated side chains as in other highly substituted polymers. The calculation of the average *d*-spacing increment is in reasonable agreement with the noninterdigitated bilayer model.

We next address the question of side-chain tilting. The width of the backbone plus the non-alkyl portion of the side chain could be estimated from the intercept of the linear $d-n$ plot, (Figure 10a). The extrapolated intercept of the *d* vs *n* plot at the ordinate axis was 7.15

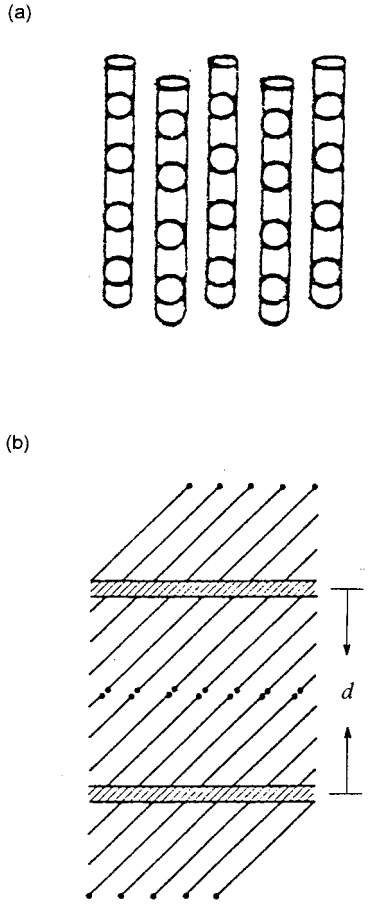

Figure 9. Schematic representations of the (a) zigzag model and (b) tilted side chains between main chains proposed by Wegner.

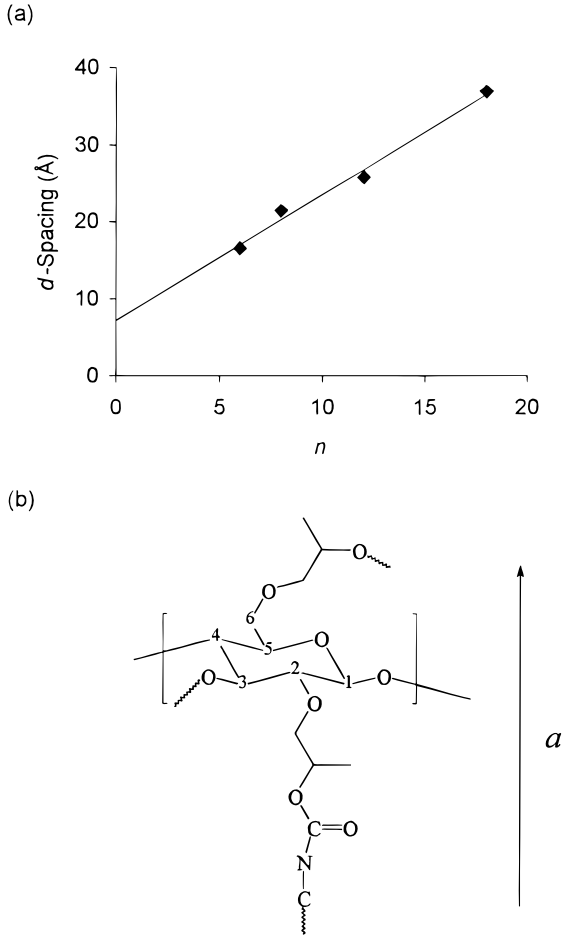

Figure 10. (a) $d-n$ plot of the solvent-cast C*n*HPC's. (b)-Theoretical representation of the projected length in the *a* direction.

Å. As illustrated in Figure 10b, the projected length in the *a*-direction from the C2 position on the ring to the C−N bond next to the urethane linkage was 8.30 Å. Together with the ring thickness and the projected length of the substituent on the C6 position, the total projected length in this direction was much greater than the extrapolated intercept. This would suggest that the side chain, or portions of it, must be tilted at an angle to the main-chain normal.

(b) Sheared C12HPC and C18HPC. The effects of shear on structural development were examined by slowly cooling the sheared sample on a hot stage without annealing (process 1). The notations C12-S and C18-S will be used to represent the samples prepared by this process. Samples prepared by process 2 (annealed in the molten state) presumably had erased the shear effect and were denoted as C12-ns and C18-ns, respectively. Samples fast-cooled from the molten state after annealing (process 3) are designated as C12-fc and C18-fc, respectively. The same notations were adopted for the samples examined by POM.

The odd-ordered diffraction patterns in the low-angle region were retained in the sheared samples which, according to Wegner's model, could indicate that the main chains were assembled in a zigzag fashion. However, the *d* spacings of the primary reflections for all three sheared samples were greater than those of the as-prepared samples. For C12HPC, the *d* spacing increased from 27.6 Å in the bulk sample to 29.1−29.9 Å in the sheared samples, depending on the cooling process. A more prominent increase in *d* spacing, from 37.1 to 39.5 Å, was obtained when the bulk C18HPC was sheared. Similar observations had been reported in other alkyl-substituted polymers in the literature.[8,9] The increase in *d* spacing, as the samples underwent various heating/cooling cycles, could be attributed to the disordering and reorganization of alkyl side chains which acted as spacers between neighboring main chains. A detailed investigation on the crystal structures of *n*-paraffins by Müller[27] indicated that paraffin crystals would have the largest expansion in the *a*-axis as the sample was heated. Since the *d* spacing of alkyl-substituted polymers depends largely on the length of alkyl side chains, disordering and expansion of the alkyl side chains in turn could result in increases in the *d* spacings of the polymers.

The diffraction profile of the C18-S sample was rich in structural information. The results appeared to suggest two sets of *d* spacings, one set with primary reflection at 39.5 Å together with third order at 13.9 Å and fifth order at 8.4 Å, and the other set having first-order reflection located at 35.5 Å and second order at 18.0 Å. It is interesting to note that the DSC heating trace of C18-S manifested two side-chain melting peaks at 37 and 57 °C, respectively, and WAXS study of C18-S exhibited characteristic reflections of both α_H (α-hexagonal phase) and β_T (β-triclinic phase) crystalline forms of long-chain hydrocarbons.[23] Müller had shown, in WAXS studies of $C_{18}H_{38}$ and $C_{20}H_{42}$, the coexistence of α_H (4.2, 2.4, and 2.1 Å) and β_T (4.5, 3.8, and 3.6 Å) crystalline modifications.[27] Since the side chains in our polymers organize themselves in multiple crystalline modifications, the two sets of *d* spacings in C18-S become understandable.

For C18HPC cooled by process 2, in which the effect of shear had been largely eliminated by conditioning the sample in the molten state, the *d* spacings also appeared to come from two different layered structures. In the first set of spacings, the peak at 35.2 Å was the major reflection and the second-order peak at 17.9 Å was clearly seen. In the second set, the previously observed peak at 39.5 Å in process 1 now was weak in intensity but the third order at 13.9 Å remained visible. The assignment of two sets of *d* spacings was further supported by the WAXS studies of the partially alkyl-substituted HPC.[28] As we carefully examined the reflections of the C18-ns sample in the wide-angle region, we found a broad diffraction peak at 4.2 Å (α_H), a strong peak at 3.9 Å, and a shoulder at 4.5 Å (β_T).[23] The two co-existing side-chain organizations are again consistent with two sets of *d* spacings in the low-angle region. However, elimination of the shear effect apparently favored the layered structure with the shorter primary *d* spacing and, at the same time, the formation of β_T modification in the alkyl side chains. For the C18-fc sample, the periodicity of chain packing was identified only by a single reflection at 38.6 Å, with no higher order reflections. Compared to the reflections of S and ns samples in the low-angle region, the peaks of the fast-cooled sample were broader and the intensities were much weaker, indicating a less ordered packing of the main chains.

We had shown in a previous publication[23] that the quenched C12HPC specimen had unexpectedly high side-chain melting enthalpy, higher even than that of the sheared C12HPC (C12-S). If we consider the fast-cooling process (ca. 50 °C/min) adopted in the WAXS experiment to be comparable to the quenching process in the DSC experiment, the C12-fc sample should have the shortest *d* spacing compared to C12-S and C12-ns, due to the fact that the C12-fc sample had the highest value of side-chain melting enthalpy in DSC study;[23] hence, the structure should be most compact. As seen in Table 2, the C12-fc sample did exhibit the smallest *d* spacing among the three thermally treated C12HPC samples, which suggested a relationship between side-chain and main-chain organizations. To ascertain this assumption, an additional WAXS experiment of C12HPC sample cooled from the molten state at a rate of 10 °C/min, which showed no side-chain melting endotherm in the DSC heating scan, was performed. A larger *d* spacing would be thus expected according to our reasoning, and indeed, this sample displayed a large *d* spacing (30.8 Å). Thus, the correlation between layer spacing and side-chain order is clearly demonstrated.

Morphology Studies. (a) Substituent Effect on Polymer Morphology. In the micrographs of the solvent-cast samples, spherulitical morphology was clearly observed for C6HPC, Figure 5a. In Figure 5b, a spherulite was found embedded in the weakly birefringent background for C8HPC. On the other hand, C12HPC and C18HPC exhibited branched lamellar structure and mottled texture, respectively; the latter was characteristic of a liquid crystalline structure.[25] As seen in Figure 4, C6HPC and C8HPC each displayed a broad melting peak which was typical of conventional crystalline polymers. The sharp endothermic peaks of C12HPC and C18HPC, however, were commonly observed in the isotropization of liquid crystalline polymers. Thus, the DSC results are consistent with morphological observations. In addition, the magnitude of undercooling (ΔT), which was defined as the temperature difference between the isotropization temperature (T_i) in the first heating (thermograms not shown) and T_{exo} in the cooling scans, showed different trends for the four polymers. C6HPC and C8HPC had a ΔT of 30 °C, whereas C12HPC and C18HPC exhibited smaller ΔT's of ca. 13 and 18 °C, respectively. Furthermore, the T_{exo}'s of C12HPC and C18HPC showed little dependence on the cooling rate. The narrow isotropization peaks, the small magnitude of ΔT, and the slight cooling-rate dependence of T_{exo} are all characteristic of liquid crystalline polymers. Putting together the POM observations with DSC results, we conclude that C6HPC and C8HPC are crystalline polymers but C12HPC and C18HPC are liquid crystalline polymers.

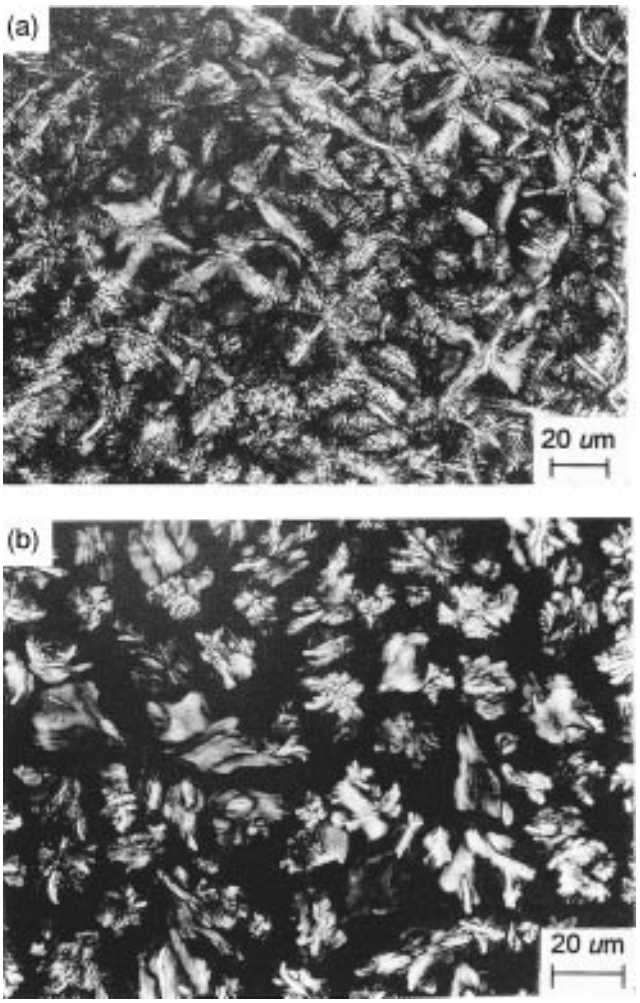

Figure 11. Optical micrographs of the annealed (a) C12HPC and (b) C18HPC after slow cooling from the melt.

(b) Shear Effect on Polymer Morphology. We had shown in the WAXS study that the sheared samples exhibited better ordered diffraction profiles than the samples with no shear. Therefore, different morphologies between the S and ns samples were expected from optical microscopy. Indeed, the sheared and the annealed samples displayed different textures. The spherulite-like structure[29,30] in the sheared C12HPC (Figure 6a) was no longer observed in the annealed sample (Figure 11a), which displayed a birefringent texture of no particular pattern. The annealed C18HPC (C18-ns) exhibited a loose structure, Figure 11b, which bore little resemblance to the nematic LC morphology in the sheared sample, Figure 8a. That the shearing process accentuates the development of a more ordered morphology, by the observation of optical microscopy, is

clearly illustrated. The POM observation supports the WAXS results with regard to the development of a more ordered structure induced by shear.

(c) Phase Transitions in C12HPC and C18HPC. The observation of crystalline textures at high temperatures in the step-cooling experiments was puzzling because, according to conventional wisdom, the transition from the isotropic to the liquid crystalline state was always thought to occur at a higher temperature than the transition from the liquid crystalline state to the crystalline state. The only exception, to our knowledge, was a recent study by Keller and co-workers,[25] who observed experimentally by *microscopy* that poly(*n*-(4,4′-biphenyl)-2-chloroethane) could, under certain conditions, crystallize at temperatures above the T_i determined by DSC. Our experiments were designed primarily on the basis of Keller's phase diagram and the thought that the application of shear would accentuate the development of liquid crystalline structures. When C18HPC was step-cooled from the molten isotropic state, an axialitic morphology was observed at 109 °C, only 6 °C below the isotropization temperature in the DSC heating scans and 12 °C above the exotherm temperature (97 °C) in the cooling scan. It seemed, therefore, that crystalline structures (admittedly minor in amount) were able to develop if the crystallization temperature and the cooling rate were carefully selected. In the present case, crystalline texture was detected only by maintaining the sample temperature close to the DSC isotropic melting point; accordingly, these crystalline structures were kinetically metastable. Our observation is in agreement with the results of Keller.

As the temperature was lowered to 102 °C, a nematic structure appeared in C18HPC. Taking into account the temperature difference resulting from the different cooling rates used in the POM and DSC experiments, the temperature for the observation of the nematic structure in POM can be regarded as being coincident with the exothermic temperature in the corresponding DSC cooling scan. The size of the crystals and the birefringence intensity of the nematic structures continued to increase as the polymer underwent the exothermic transition in the DSC cooling scan. The exothermic peak then represented the transition from the isotropic to the liquid crystalline state. As the temperature was lowered further, there was no evidence of additional exothermic event which could be assigned as the liquid-crystalline-to-crystalline (LC → C) transition in the DSC cooling scans or morphological changes visible on the level of optical microscopy which would indicate a LC → C transformation.

C12HPC exhibited a similar phase transition pattern to that of C18HPC. As the sample was step-cooled from the molten state, a leaflike texture developed at 99 °C. This leaflike structure was also found to be a crystalline structure, due to the fact that the rotation of the observed birefringence followed exactly the rotation of the POM sample platform. Similar to the observation in C18HPC, this crystalline leaflike texture of C12HPC was observed in POM at only 6 °C below the isotropization temperature (105 °C) in the DSC heating scan. As the temperature was lowered further, a less ordered second structure appeared at 94 °C, which corresponded to the exothermic peak in the DSC cooling scan. By the same reasoning as the one used for C18HPC, the exothermic transition in the DSC cooling experiment was attributed to the isotropic-to-liquid-crystalline transition. The phase transition temperatures for C12HPC and C18HPC are summarized in Figure 12; morphology development in the temperature spans between T_m and T_i is kinetically controlled in this scheme, in accordance with Keller's reasoning.

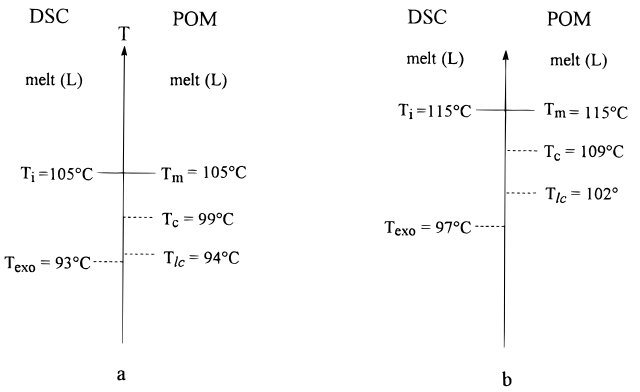

Figure 12. Phase transition temperatures of (a) C12HPC and (b) C18HPC, in which T_{lc} is the temperature at which the LC texture observed in POM. The solid and the dotted lines represent the transition temperatures in the heating and cooling scans, respectively.

(d) Effect of Cooling Rate on Morphology Development. According to the diagram of phase transition temperatures depicted in Figure 12, crystallization of C12HPC and C18HPC from the melt might be retarded or bypassed if the cooling rate was sufficiently fast so that only the transition to LC phases could be observed. The following experimental findings supported this assertion. When the sheared C12HPC sample was cooled from the melt at a rate of 10 °C/min, the optical micrograph displayed an intense birefringent texture which seemed to be a combination of the smaller and less regular leaflike features and the second structure (compared Figure 6b−d with Figure 7b). When the same sheared sample was fast-cooled from the melt (C12-fc), however, only Schlieren liquid crystalline texture was seen. Obviously, the degree of order of the sheared C12HPC decreased as the cooling rate increased. The effect of cooling rate on morphology development was more pronounced in the series of experiments with sheared C18HPC. A visually loose nematic structure was observed when sheared C18HPC was cooled at 10 °C/min from the melt. In contrast, the sample exhibited only a weakly birefringent fine-grain structure, when fast-cooled from the melt (C18-fc). Poor order in the fc samples was confirmed by subsequent heating experiments. The thus pretreated C12HPC and C18HPC started to lose birefringence at lower temperatures and samples eventually became isotropic at 102 and 113 °C, respectively, the same temperatures at which the liquid crystalline second structures in the slow-cooled samples lost the Schlieren and fine-grain textures (Schemes 1 and 2). The cooling-rate effect on morphology development seen by POM again was confirmed by WAXS studies which displayed no higher order reflections in the low-angle region for C18-fc and only a weak third-order peak for the 12-fc sample.

Conclusions

A series of alkyl-substituted semiflexible polymers were synthesized by reacting HPC with hexyl, octyl, dodecyl, and octadecyl isocyanates. All the C*n*HPC's showed odd-order reflections in the low-angle region of the WAXS profiles except that C18HPC also exhibited a second-order reflection. A bilayer model was proposed

in which the main chains were aligned in a zigzag fashion and the alkyl side chains were not interdigitated but were tilted at an angle to the main-chain normal.

Polymer morphology was influenced by the alkyl substituents. C6HPC and C8HPC were crystallizable, but C12HPC and C18HPC displayed liquid crystalline textures. Shear in the molten state induced better ordered liquid crystalline structures, namely, a "spherulite-like" texture for C12HPC and a nematic liquid crystalline morphology for C18HPC. Crystalline structures, although only a minor fraction of the total mass, developed when the samples were very slowly cooled from the isotropic state. A diagram of phase transition temperatures for each polymer was constructed based on the POM observation and the DSC data.

Acknowledgment. We gratefully acknowledge the support of this investigation by the National Science Foundation, Division of Materials Research, Grants 9201003 and 9424317. Acknowledgment is also made to the donors of the Petroleum Research Fund, administered by the American Chemical Society, for the support of this study. Thanks are also due to TA Instruments for providing the modulated calorimetric instrument for this research.

References and Notes

(1) Jones, A. T. *Makromol. Chem.* **1964**, *71*, 1.
(2) Jordan, E. F.; Feldeisen, D. W.; Wrigley, A. N. *J. Polym. Sci. A-1* **1971**, *9*, 1835.
(3) Jordan, E. F. *J. Polym. Sci., Polym. Chem.* **1972**, *10*, 3347.
(4) Platé, N. A.; Shibaev, V. P.; Petrukhin, B. S.; Zubov, Y. A.; Kargin, V. A. *J. Polym. Sci. A-1* **1971**, *9*, 2291.
(5) Morawetz, H.; Hsieh, H. W. S.; Post, B. *J. Polym. Sci., Polym. Phys.* **1976**, *14*, 1241.
(6) Majnusz, J.; Catala, J. M.; Lenz, R. W. *Eur. Polym. J.* **1983**, *19* (10/11), 1043.
(7) Ballauff, M.; Schmidt, G. F. *Mol. Cryst. Liq. Cryst.* **1987**, *147*, 163.
(8) Duran, R.; Ballauff, M.; Wenzel, M.; Wegner, G. *Macromolecules* **1988**, *21*, 2897.
(9) Rodriguezz-Parada, J. M.; Duran, R.; Wegner, G. *Macromolecules* **1989**, *22*, 2507.
(10) Kricheldorff, J. H.; Domschke, A. *Macromolecules* **1996**, *29*, 1337.
(11) Berger, K.; Ballauff, M. *Mol. Cryst. Liq. Cryst. Inc. Nonlin. Opt.* **1988**, *157*, 109.
(12) Steuer, M.; Horth, M.; Ballauff, M. *J. Polym. Sci., Polym. Chem.* **1993**, *31*, 1609.
(13) Kricheldorff, J. H.; Domschke, A. *Macromolecules* **1994**, *27*, 1509.
(14) Wendorff, J. H.; Hermann-Schonherr, O. *Makromol. Chem. Rapid Commun.* **1986**, *7*, 791.
(15) Tashiro, K.; Ono, K.; Minagawa, Y.; Kobayashi, M.; Kawai, T.; Yoshino, K. *J. Polym. Sci., Polym. Phys.* **1991**, *29*, 1223.
(16) Chen, S.-A.; Ni, J.-M. *Macromolecules* **1992**, *23*, 6081.
(17) Hsu, W.-P.; Levon, K.; Ho, K.-S.; Myerson, A.; Kwei, T. K. *Macromolecules* **1993**, *26*, 1318.
(18) Zheng, W.-Y.; Levon, K.; Laakso, J.; Osterholm, J.-E. *Macromolecules* **1994**, *27*, 7554.
(19) Guo, J.-X.; Gray, D. G. *Macromolecules* **1989**, *22*, 2082.
(20) Yim, C. T.; Gilson, D. F. R.; Kondo, T.; Gray, D. G. *Macromolecules* **1992**, *25*, 3377.
(21) Dave, V.; Frazier, C. E.; Glasser, W. G. *J. Appl. Polym. Sci.* **1993**, *49*, 1671.
(22) Dave, V.; Glasser, W. G. *J. Appl. Polym. Sci.* **1993**, *48*, 683.
(23) Lee, J. L.; Pearce, E. M.; Kwei, T. K. *Macromolecules* **1997**, *30*, 6877.
(24) Woodward, A. E. *Atlas of Polymer Morphology*; Hanser: 1988; Chapter VII.
(25) Heberer, D.; Keller, A.; Percec, V. *J. Polym. Sci., Polym. Phys.* **1995**, *33*, 1877
(26) Skoulios, A. E. *Sagamore Conf. Proc.* **1973**, 121.
(27) Müller, A. *Proc. R. Soc. London, Ser. A* **1930**, *127*, 417.
(28) Lee, J. L.; Pearce, E. M.; Kwei, T. K. submitted to *Macromol. Chem. Phys.*
(29) Chang, S. Z. D.; Lee, S. K.; Barley, J. S.; Hsu, S. L. C.; Harris, F. W. *Macromolecules* **1991**, *24*, 1883.
(30) Han, H.; Bhowmik, P. K. *Polym. Prep.* **1995**, *36* (2), 329.

MA970647C